表2　抗HIV療法の初回療法における推奨選択薬と選択時の留意事項

Table 3. Recommended Components of Initial Antiretroviral Therapy and Considerations for Choosing a Regimen

Component	Considerations for Choice	Major Toxic Effects and Cautions
Nucleoside reverse transcriptase inhibitors[a]		
Tenofovir/emtricitabine[b,c]	Well tolerated Efficacy superior to zidovudine/lamivudine[4,62] and similar to stavudine/lamivudine[63] Available as a once-daily fixed dose	Baseline renal function should be evaluated before initiating tenofovir Reduce dose or avoid in patients with renal dysfunction
Abacavir/lamivudine[d]	Noninferior to tenofovir/emtricitabine in 1 trial[10] May have less activity in patients with viral load ≥100 000 HIV RNA copies/mL[63] Available as a once-daily fixed dose	Hypersensitivity syndrome in 5% to 8% of persons (risk associated with HLA-B*5701 genotype) Risk reduced with HLA-B*5701 screening[64,65] May be associated with increased risk of myocardial infarction[14,15]
Nonnucleoside reverse transcriptase inhibitors[e]		
Efavirenz	Standard-of-care comparator in many trials Available as a once-daily fixed dose with tenofovir/emtricitabine	Central nervous system toxicity may be limiting Potentially teratogenic in first trimester of pregnancy Associated with lipoatrophy when given with thymidine reverse transcriptase inhibitors[20]
Ritonavir-boosted protease inhibitors[f]		
Lopinavir	Substantial clinical trial data and phase 4 experience supporting efficacy Heat-stable tablet 1 or 2 doses per day for treatment-naive patients	Gastrointestinal adverse effects Hyperlipidemia, especially hypertriglyceridemia
Atazanavir	Noninferior to ritonavir-boosted lopinavir Less hyperlipidemia and diarrhea[66] Once-daily dosing	Hyperbilirubinemia (UGT1A1-28 alleles and T3435C polymorphism in *MDR1* gene) Occasionally associated with nephrolithiasis Acid-reducing agents decrease atazanavir concentrations; proton pump inhibitors should be used cautiously
Fosamprenavir	Noninferior to ritonavir-boosted lopinavir[13] Once-daily or twice-daily dosing possible; more robust data with twice-daily dose	Similar adverse effect profile to ritonavir-boosted lopinavir Rash
Darunavir	Noninferior to ritonavir-boosted lopinavir and superior in those with viral load ≥100 000 HIV RNA copies/mL Less nausea, lower triglyceride levels[65] 800 mg + 100 mg ritonavir once daily	Rash
Saquinavir	Noninferior to ritonavir-boosted lopinavir, with lower triglyceride levels.[67] Twice-daily dosing	High pill burden

[a] Zidovudine/lamivudine is considered an alternative. [b] A baseline urinalysis and estimation of creatinine clearance or glomerular filtration rate for assessment of renal function are recommended. All patients receiving tenofovir should be observed for development of renal dysfunction. [c] Or lamivudine. [d] Or emtricitabine. [e] Nevirapine (in women with <250 CD4 cells/μL and men with <400 CD4 cells/μL) is considered an alternative. [f] Substantial clinical trial data exist for ritonavir-boosted lopinavir as initial antiretroviral therapy, including data on long-term outcomes. Each of the other ritonavir-boosted protease inhibitors has been compared with ritonavir-boosted lopinavir but not with one another. Choice of ritonavir-boosted protease inhibitor should be individualized.

たいていは、まず、エファビレンツ、またはリトナビルで作用増強したプロテアーゼ阻害薬のいずれかを選び、次に、2種類の核酸系逆転写酵素阻害薬(テノホビルとエムトリシタビンの合剤またはアバカビルとラミブジンの合剤のいずれか)を選んで組み合わせる。治療の失敗を発見すれば迅速に対処することが肝要であり、すでに何度も薬剤変更を行わざるを得なかった患者においても、治療の目標は、血中のウイルス量を測定検出限界値未満に抑え続けることである。

解説

HIV感染症の次なる新しい時代の幕開け

白阪琢磨　国立病院機構大阪医療センター HIV/AIDS先端医療開発センター センター長

1981年に報告されたAIDSの病原体であるHIVを83年に世界で初めて発見したモンタニエ博士らは、その功績で2008年ノーベル医学・生理学賞を受賞した。1996年ごろに現在の抗HIV療法が登場し、HIV感染症は慢性疾患ととらえられるまでになった。

今回、紹介する2つの論文は、HIV感染症の分野

で新たな進展につながるものである。

まず、Hall博士らの論文では、HIV感染が早期かどうかを鑑別できるBEDアッセイと呼ばれる診断技術を疫学に応用したものである。HIVに感染すると血中にHIVに対する抗体が産生されるが、抗体の血中レベルは時間の経過とともに上昇し、ある程度以上からは定常状態になると言われている。HIVは多くの変異があり、サブタイプも多く知られている。BEDアッセイではサブタイプB、-E、Dに対するIgGを血中の総IgGとの相対値で測定し、基準値以下なら感染の早期と推定でき、HIV感染後、血中に抗体ができて平均156日以内の感染を診断できるという。

本研究では2006年に米国22州の13歳以上の新規感染報告者(報告時および報告後半年以内にAIDSと診断された患者は除く)を対象に、利用可能な保存血を用いてBEDアッセイを実施したところ、31%が最近の感染であった。米国ではHIV陽性と診断されると、HIV/AIDSサーベイランスの訓練を受けた専門家が感染経路を含む詳細なデータを患者から聴取する。このためHIV感染疫学のデータの信憑性は高いとされており、本論文でも年齢別、性別、人種別はもちろん、感染経路別の推移も有益な情報と言える。

本論文では、2006年の新規感染報告者の各カテゴリー別に感染早期感染者数を計算し(表1)、さらに2003～06年の過去4年間の逆解析を行い、1977年以降に拡大した推定も試みている。それによれば、1984～85年をピークとする新規感染者は91年ごろには半減し、以降漸増傾向に移行した。この傾向は性別では男性に顕著であり、感染経路別では男性同性間性的接触者(MSM: men who have sex with men)で認められた。他方、異性間性的接触者では1988～99年にゆるやかなピークを形成した以降は漸減傾向が観察された。米国に多く報告されていたIDU(注射薬物乱用者)での感染者数は91年ごろには大きく減少し、それ以降は漸減傾向が認められている。今後はBEDアッセイの導入で感染早期の感染者を診断でき、HIV感染の予防対策の立案と評価が、より詳細に行えると期待される。

次に、Hammer博士らの論文は、国際AIDS学会所属の米国HIV専門医師14人が、2006年に*JAMA*で提唱した成人HIV感染症に対する抗HIV療法のガイドラインを改訂したものである。Hammer博士らは1996年に同ガイドラインを提唱して以来、隔年で改訂を行ってきた。今回の大きな改訂点として、治療開始時期が早まったことと、推奨レジメンの変更があげられる。これまで初回療法の開始は臨床症状やCD4値、血中のウイルス量などを基準に決定されてきた。特に、CD4値が重要な基準である。現在の抗HIV療法が始まった1996年ごろは、CD4値が500個/μL未満で開始を勧められたが、その後、200個/μL未満までに低下し、今回は350個/μL未満が提唱されている。開始時期は、薬剤開発の状況や、出現する副作用、臨床知見などを根拠に変更されてきた。今回、新たなプロテアーゼ阻害薬、非核酸系逆転写酵素阻害薬に加えて、全く新しいクラスに属するインテグラーゼ阻害薬やCCR5阻害薬が米国で承認された。これらの新薬は従来の薬剤と比べて現時点で副作用報告が少なく、抗HIV療法の有効性と安全性への信頼性が高まり、抗HIV薬の合剤など飲みやすさにも配慮した製剤開発は、服薬の早期導入を可能とした。また、最近、CD4値が高い未治療者でもウイルス量が観察される例では、AIDS指標疾患以外の悪性腫瘍の合併や心血管障害、肝障害、腎障害の合併が報告され、CD4値が350個/μL以上でも非感染者より死亡率の高いことなどが示され、350個/μL未満では初回療法の開始を強く勧めている。選択薬剤の推奨については表を参照されたい。新規に承認されたインテグラーゼ阻害薬はまだ初回療法に掲載されていないが、未治療患者を対象とした同薬の臨床試験データの結果によっては、初回療法の選択薬となると予想される。このように、推奨選択薬も当面は目まぐるしく改訂され続けると考えられる。HIV感染症の治療を担当する医師は、ガイドラインなどのアップデートに常に対応する必要がある。

Scand J Plast Reconstr Surg Hand Surg, 2008; 42: 105–107

informa
healthcare

CASE REPORT

Suspected case of primary malignant melanoma of the parotid gland

ARATA TSUTSUMIDA[1], YUHEI YAMAMOTO[1], MITSURU SEKIDO[1] & TOMOO ITOH[2]

[1]*Department of Plastic and Reconstructive Surgery,* [2]*Department of Surgical Pathology, Hokkaido University, Sapporo, Japan*

Abstract

A patient presented with malignant melanoma of the parotid gland with no obvious primary lesions, which was treated by total parotidectomy with excision of skin. Despite radiotherapy for brain metastases and combination chemotherapy for lung and lymph node metastases, she died 13 months after the initial operation.

Key Words: *Melanoma, parotid gland, chemotherapy, radiotherapy*

Introduction

Melanomas that involve the parotid gland are unusual, and primary melanoma of the parotid is extremely rare and characterised by difficult and late diagnosis and classification. Most previously reported cases have presented as metastatic lesions, often from cutaneous melanoma elsewhere in the head and neck.

We describe a 63-year-old woman who had a malignant melanoma of the parotid gland without obvious primary lesions at the time of initial presentation.

Case report

A 63-year-old woman presented with a swelling in the left parotid region that had developed over two years. On examination there was a nodular lesion about 3 cm in diameter, of firm to elastic consistency, and adherent to the superficial and deep tissues, causing no pain. The overlying skin was reddish, but there were no signs of facial nerve palsy (Figure 1). No metastatic regional lymph nodes were found in the neck. Preoperative investigations included fine needle aspiration cytology, chest radiograph, computed tomography (CT) from the head to the pelvis, and a radioisotopic scintigram. The cytology was interpreted as possibly adenocarcinoma, and the CT of the chest showed two lesions in the lung. The patient was therefore diagnosed as having a T3N0M1 parotid carcinoma on the UICC classification. Though there were lung metastases, we planned to excise the large parotid tumour, and then resect the lung metastases as a palliative procedure.

We did a total left parotidectomy involving the zygomatic, buccal, and marginal mandibular branches of the facial nerve together with the excision of overlying skin with a 1-2 cm margin from the reddish area. Initially, the frozen sections of the primary tumour showed adenocarcinoma with no metastases in the upper neck lymph nodes, so we did not do a neck dissection. The defect was reconstructed with the free anterolateral thigh flap and the nerve was reconstructed by grafting of the cutaneous branch of the femoral nerve.

Histopathological examination showed a malignant melanoma with a well-demarcated interface between the tumour and the adjacent parotid tissue (Figure 2*a*). The tumour was composed of a generally diffuse arrangement of cells with abundant eosinophilic cytoplasm, large pleomorphic nuclei, and melanin granules (Figure 2*b*). Immunohistochemically the tumour stained for S-100 protein

Correspondence: Arata Tsutsumida, MD, PhD, Department of Plastic and Reconstructive Surgery, Graduate School of Medicine, Hokkaido University, Kita 15, Nishi 7, Kita-ku Sapporo, 060-8638, Japan. Tel: +81-11-706-6978. Fax: +81-11-706-7827. E-mail: tsutsu@med.hokudai.ac.jp

(Accepted 28 April 2006)

ISSN 0284-4311 print/ISSN 1651-2073 online
DOI: 10.1080/02844310601004707

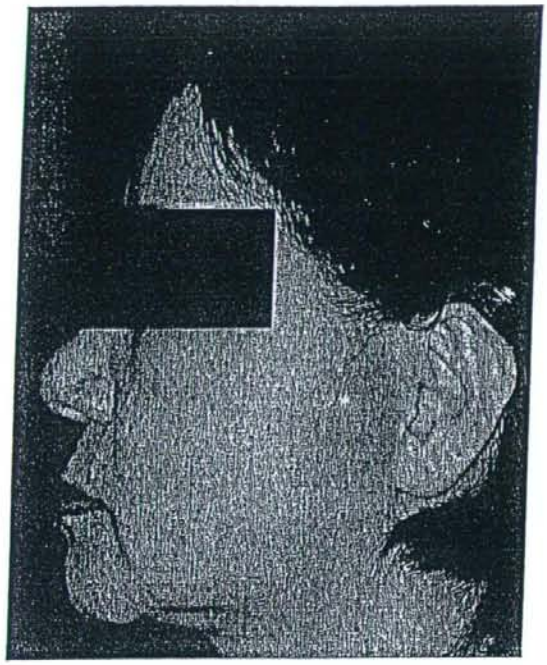

Figure 1. Presentation showing a firm nodule about 3 cm in diameter, adherent to the superficial and deep tissues in the preauricular region. The overlying skin was reddish, but there were no signs of facial nerve palsy.

(Figure 3*a*) and HMB-45 (Figure 3*b*), but not for cytokeratin. We found no other lesions in the head and neck, and she had no history of previous excisions of melanomas or pigmented lesion.

Although we had planned to excise the lung metastases, multiple brain metastases and metastases in the para-aortic lymph nodes were found after the initial operation, so she was given radiotherapy (20–25 Gy to one lesion and whole brain irradiation of 30 Gy), and two courses of the combined chemotherapy with dacarbadine (220 mg/cm^2, day 1–3), cisplatin (25 mg/cm^2, day 1–3), adriamycin (50 mg/cm^2, day 1), tamoxifen (20 mg, day 1–28), and IFN- (6 MIU, day 4–8). The VP-16 (etoposide) was given orally between courses based on the results of the collagen gel droplet embedded culture drug sensitivity test (CD-DST). The effect of combined treatment was a complete response for the para-aortic lymph node metastases, partial response for the brain and lung metastases, and stable disease for her adrenal metastases.

She died 13 months after the initial operation.

Discussion

The most common cause of malignant melanomas involving the parotid gland are metastases from other sites. Primary melanoma of the parotid gland is extremely rare, and comprises 0.68% of malignant neoplasms of the parotid gland [1].

The possibility of a parotid melanoma being considered as a primary tumour is questioned by some authors [2]. However, theoretically, a melanoma could arise from there. Takeda reported that melanocytes can exist in the interlobular duct of the parotid gland [3], and these could potentially serve as cells of origin for a primary malignant melanoma of the gland.

It is difficult to diagnose a melanoma of the parotid gland because of the lack of pigmentation and atypical histology. In the series reported by Wang et al. [4], 3 of 19 patients were initially misdiagnosed as having some other form of carcinoma. This distinction can be particularly problematic in tumours that are poorly differentiated and generally amelanotic. In such cases,

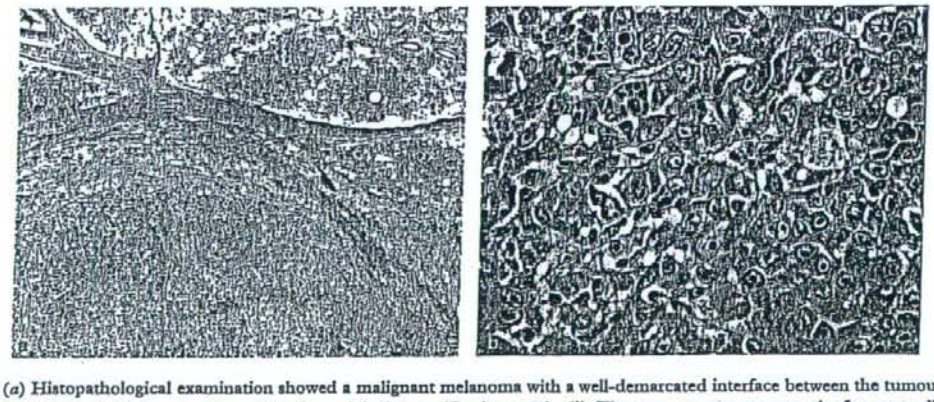

Figure 2. (*a*) Histopathological examination showed a malignant melanoma with a well-demarcated interface between the tumour and the adjacent parotid gland (haematoxylin and eosin, original magnification ×40). (*b*) The tumour was composed of a generally diffuse arrangement of cells with abundant eosinophilic cytoplasm, large pleomorphic nuclei, and melanin granules (haematoxylin and eosin, original magnification ×200).

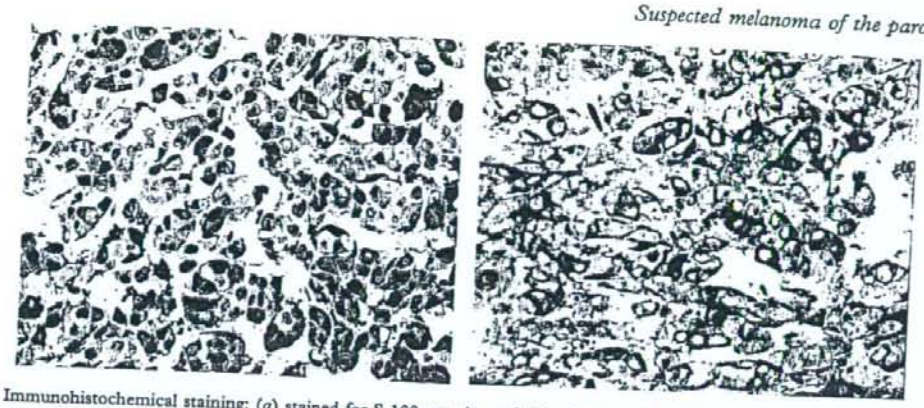

Figure 3. Immunohistochemical staining: (*a*) stained for S-100 protein, and (*b*) stained for HMB-45.

immunohistochemistry can be helpful. In our case we found melanin granules and immunostaining with anti S-100 protein and anti HMB-45 antibody.

It is also difficult to diagnose whether the melanoma is a primary or secondary lesion. Metastases involving the intraparotid lymph nodes tend to have well-demarcated interfaces between the capsule of the node and the adjacent salivary gland tissue, in contrast to supposed primary melanomas that tend to infiltrate with poor demarcation [5]. Based on this argument, our patient may have had a metastatic melanoma. Woodward et al. [6] proposed that four conditions should be met before making a diagnosis of primary malignant melanoma of the parotid: the bulk of the tumour should be within the parotid gland; the tumour should contain no identifiable lymph node tissue; there should be no evidence of melanoma elsewhere in the body; and there should be no evidence of previous excision of melanoma or progression of a pigmented lesion. Our case met the first three criteria. It is not possible to diagnose the lung lesions as primary and the lesion of the parotid gland as secondary.

As far as treatment is concerned, a study of published papers seems to suggest the need for total parotidectomy [2], though some authors have suggested that such a radical intervention would not influence life expectancy because of the poor prognosis of such a tumour. Partial parotidectomy is considered insufficient because of the high risk of recurrence [7]. The issue of whether the neck dissection should be done or not is still controversial, though Vaglini et al. recommend the neck dissection because of the high incidence of hidden metastases in the nodal groups [8]. At present the conclusions could be drawn on the type of tumour and its staging [9].

Radiotherapy is generally considered to be of limited value, and chemotherapy has not been shown to offer particular benefit in terms of an improved prognosis. We previously reported that the median survival period after metastases from a melanoma was eight months [10], but in our case radiotherapy for brain metastases (partial response for seven months) and combined chemotherapy was effective.

References

[1] Bahar M, Anavi Y, Abraham A, Ben-Bassat M. Primary malignant melanoma in the parotid gland. Oral Surg Oral Med Oral Pathol 1990;70:627–30.

[2] Renaut AJ. Melanoma arising within the parotid salivary gland – a case report and review of management. Eur J Surg Oncol 1996;22:201–2.

[3] Takeda Y. Melanocytes in the human parotid gland. Pathol Int 1997;47:581–3.

[4] Wang BY, Lawson W, Robinson RA, Perez-Ordonez B, Brandwein M. Malignant melanoma of the parotid. Arch Otolaryngol Head Neck Surg 1999;125:635–9.

[5] Greene GW Jr, Bernier JL. Primary malignant melanomas of the parotid gland. Oral Surg 1961;14:108–16.

[6] Woodward RT, Shepard NA, Hensher SR. Malignant melanoma of the parotid gland: a case report and literature review. Br J Oral Maxillofac Surg 1993;31:313–5.

[7] Martins AS, Souza AL, Souza LS, Laqe HT. Surgical procedures for primary, metastatic or adjacent parotid tumours. Int Surg 1999;84:318–25.

[8] Vaglini M, Belli F, Santinami M. The role of parotidectomy in the treatment of nodal metastases from cutaneous melanoma of the head and neck. Eur J Surg Oncol 1990; 16:28–32.

[9] Jecker P, Hartwein J. Metastasis to the parotid gland: is a radical surgical approach justified? Am J Otolaryngol 1996; 17:102–5.

[10] Tsutsumida A, Yamamoto Y, Sugihara T. Analysis of melanoma patients with distant metastases. J Jpn Plast Reconstr Surg 2004;24:483–6.

Pediatrics International (2008) **50**, 806–809 doi: 10.1111/j.1442-200X.2008.02650.x

Original Article

Detection of a novel silent deletion, a missense mutation and a nonsense mutation in *TCOF1*

Hirotaka Fujioka,[1,2,3] Tadashi Ariga,[1,3] Katsumi Horiuchi,[4] Satoshi Ishikiriyama,[5] Kimie Oyama,[6] Makoto Otsu,[1] Kunihiro Kawashima,[3] Yuhei Yamamoto,[2] Tsuneki Sugihara[2] and Yukio Sakiyama[1]

[1]*Research Group of Human Gene Therapy, Departments of* [2]*Plastic Surgery and* [3]*Pediatrics, Hokkaido University Graduate School of Medicine, Hokkaido,* [4]*Department of Plastic Surgery, Sapporo City General Hospital, Sapporo,* [5]*Department of Medical Genetics, Shizuoka Children's Hospital, Shizuoka and* [6]*Department of Maxillofacial Orthognathics, Tokyo Medical and Dental University, Tokyo, Japan*

Abstract ***Background***: Treacher Collins syndrome (TCS) is a disorder of craniofacial development, that is caused by mutations in the *TCOF1* gene. TCS is inherited as an autosomal dominant trait, and haploinsufficiency of the *TCOF1* gene product treacle is proposed to be etiologically involved.

Methods: Mutational analysis of the *TCOF1* gene was done in 10 patients diagnosed with TCS using single-strand conformation polymorphism and direct sequencing.

Results: Among these 10 patients, a novel 9 bp deletion was found, together with a previously reported 2 bp deletion, a novel missense mutation and a novel nonsense mutation in three different families. Familial studies allowed judgment of whether these abnormal findings were responsible for the TCS phenotype, or not. The 9 bp deletion of three amino acids Lys-Glu-Lys (1378–1380), which was located in the nuclear localization domain of treacle, seemed not essential for the treacle function. In contrast, the novel mutation of Ala26Val is considered to affect the LisH domain, an important domain of treacle. All of the mutations thus far detected in exon 5 have resulted in frameshift, but a nonsense mutation was detected (Lys159Stop).

Conclusion: The information obtained in the present study provides additional insights into the functional domains of treacle.

Key words deletion, missense mutation, *TCOF1*, Treacher Collins syndrome, treacle.

Treacher Collins syndrome (TCS; MIM 154500) is a disorder of craniofacial development that is inherited as an autosomal dominant trait caused by heterozygous mutations in the *TCOF1* gene (MIM 606847). The features of the disorder include downward slanting palpebral fissures, coloboma of the lower eyelid, micrognathia, microtia, other deformity of the ears include the middle ear bones that can lead to conductive hearing loss, hypoplastic zygomatic arches and cleft palate. The *TCOF1* gene encodes for the protein treacle, a 1411 amino acid-protein. Treacle is a nucleolar phosphoprotein, composed of three domains with unique *N*- and *C*-termini, and a large central region of repeated amino acids motif.[1,2] The *N*-terminus contains the LisH putative domain. The *C*-terminus contains multiple putative nuclear and nucleolar localization signals (NLS and NoLS).[3,4] The two putative casein kinase phosphorylation sites are found in the same region in every repeated unit, with the exception of mouse and human exon 11. Valdez *et al.* showed that treacle was involved in ribosomal DNA gene transcription by interacting with upstream binding factor (UBF).[5] In mice, haploinsufficiency of *Tcof1* results in the depletion of neural crest cell precursors through high levels of cell death in the neuroepithelium, which results in a reduced number of neural crest cells migrating into the developing craniofacial complex.[6]

In the present study we conducted a mutation screen in *TCOF1* and discuss the functional importance of those mutations within the protein treacle.

Correspondence: Hirotaka Fujioka, MD PhD, Department of Plastic Surgery, Hokkaido University Graduate School of Medicine, Sapporo, Hokkaido, 060-8638, Japan. Email: hfujioka@med.hokudai.ac.jp

Received 7 October 2006; revised 26 July 2007; accepted 14 December 2007; published online 8 July 2008.

Methods

Ten clinically diagnosed TCS patients were registered for the *TCOF1* gene analysis study after obtaining informed consent.

Case report

Patient 1

This patient was 1 year old. He had slanting palpebral fissures, coloboma of the lid, micrognathia, deformity of the ears, hypoplastic zygomatic arches and cleft palate. Neither parent had TCS symptoms.

Patient 2

This patient was 29 years old, and had slanting palpebral fissures, coloboma of the lid, mild deformity of the ears, hypoplastic

zygomatic arches, cleft palate and hypoplasia of the mandible. Neither parent had similar features.

Patient 3

Patient 3 was 18 years old. Coloboma of the lower lids occurred to a mild degree. He had all symptoms of TCS and pectus excavatum. His parents did not have any craniofacial anomalies. He had asthma and atopic dermatitis.

Polymerase chain reaction amplification

Genomic DNA from the affected family individuals was extracted, and then the entire coding region of the *TCOF1* gene including exon–intron junctions underwent polymerase chain reaction (PCR) amplification using primers previously reported.[2,7] Primers of 5′ UTR (from nt-186 to 36) were designed (forward, 5′-CCCCTTCGCCTTGAGG-3′; reverse, 5′-GCAGATGGTGGTAGATCAGG-3′).

Single-strand conformation polymorphism

The PCR products were screened using single-strand conformation polymorphism (SSCP).[8] Briefly, 3 μL PCR products were denatured with 7 μL 95% formamide, 0.05% xylene cyanol, and 0.05% bromophenol blue, for 5 min at 94°C, and 6 μL of each product was loaded on a GeneGel Excel 12.5/24 Kit (Amersham Pharmacia Biotech, Piscataway, NJ, USA). Electrophoresis was done at 600 V, 25 mA, 90 min at 20°C or 15°C. The gels were stained using PlusOne DNA silver staining kit (Amersham Pharmacia Biotech). SSCP variants were purified, and directly sequenced in both directions using an ABI Gene Analyzer 310 (Applied Biosystems, Foster City, CA, USA). In the cases in which a differing pattern of bands was not detected on SSCP, all PCR products for the *TCOF1* gene were sequenced.

When abnormal sequences were detected, we repeatedly checked to confirm them using different PCR products.

TA cloning

The PCR products of exon 24 from patient 1 were subcloned using TA cloning kit (Invitrogen, Carlsbad, CA, USA). Transformed competent *Escherichia coli* cells were cultured, and then plasmids in the cells were purified using QIAprep Spin Miniprep Kit (Qiagen, Hiden, Germany), and were sequenced using the M13 reverse primers prepared in the TA cloning kit.

Results

We detected *TCOF1* mutations in three of 10 patients. We found two possible *TCOF1* mutations in patient 1. One was a 9 bp deletion (c.4131–4139delAAAAGAAAA; exon 24; Fig. 1a), which would lead to a deletion of Lys-Glu-Lys (p.1378K-1380Kdel). The other was a 2 bp deletion (c.1867–1868delGA; exon 12; Fig. 1b), which was expected to result in frameshift and a premature stop codon (p.D623X). Neither abnormality was found in 100 healthy control individuals, indicating that they were not common polymorphic changes. c.1867–1868delGA was previously reported as a mutation responsible for TCS.[9] Analysis of patient 1's normal parents showed that the father possessed the 9 bp deletion but not the 2 bp deletion. His mother did not have either deletion. Thus, it was indicated that the 2 bp deletion was the real causative mutation, whereas the 9 bp deletion was silent.

Patient 2 had a single base substitution (c.77C>T), predicting p.A26V (Fig. 1c). This substitution was detected in neither of her parents nor 100 healthy individuals; therefore, this is likely to be a novel causative missense mutation in the *TCOF1* gene.

Patient 3 had a novel base substitution (c.475A>T), which resulted in a nonsense mutation (p.K159X; Fig. 1d).

Discussion

In the present study we performed *TCOF1* mutation analysis for 10 patients with TCS, and detected three causative mutations. Furthermore, two unique genetic findings, which may provide insights into the functional domain of treacle, were observed.

The 9 bp deletion, detected in patient 1 and his healthy father, is located within the *TCOF1* mutational hot spot,[7] where important domains of treacle are thought to be located.[10] The amino acids Lys-Glu-Lys seem to be included in NLS, and this region could be removed due to the 9 bp deletion. Therefore, the deletion was first expected to seriously disrupt treacle function, but it actually did not. Most *TCOF1* mutations are deletions/insertions, which consequently lead to frameshift and result in premature termination. But no frameshift change is predicted by the 9 bp deletion, therefore, this deletion could be relatively benign and non-pathological for TCS. In fact, the motif scan program (Myhits; http://myhits.isb-sib.ch/cgi-bin/motif_scan) indicates that NLS would be conserved in the case of the 9 bp deletion.

In patient 2 the novel missense mutation (p.A26V) was detected. Most mutations (80%) for *TCOF1*[11] are frameshift, and, as at the time of writing, only four missense mutations have been identified: p.A41V,[12] Y50C,[13] W53R,[7] and W53C,[12] all of which were clustered at the *N*-terminus of treacle. Here we detected the fifth missense mutation of *TCOF1*, p.A26V, at the similar N-terminal area, consistent with the previous reports. Amino acid residues in this area of treacle including Ala26 are highly conserved among various species.[13] This conserved area of treacle, amino acids 5–38 (exon 1–exon 2), consists of the predicted functional domain of LisH (LIS1 homology), which is found in multiple proteins involving craniofacial phenotypes, such as lissencephaly one, oral-facial-digital I and so on, and may participate in protein dimerization[14,15] to form the structure resembling a mallet.[16] Missense mutations in the LisH domain may influence dimerization[14] to form the structure of the mallet resulting in treacle dysfunction. Further basic study would be necessary to prove this hypothesis.

p.K159X was a novel and the first nonsense mutation reported in exon 5 of the *TCOF1* gene. The truncated protein is predicted to be approximately 10% of the length of normal treacle, resulting in a defective *N*-terminus and lack of *C*-terminus.

Detection of the novel silent 9 bp deletion, the missense mutation (A26V) and the nonsense mutation (K159X) in the *TCOF1* gene in the present study provides new insights into the functional domains of treacle. Functional study of these abnormalities in treacle is necessary to obtain more definite information.

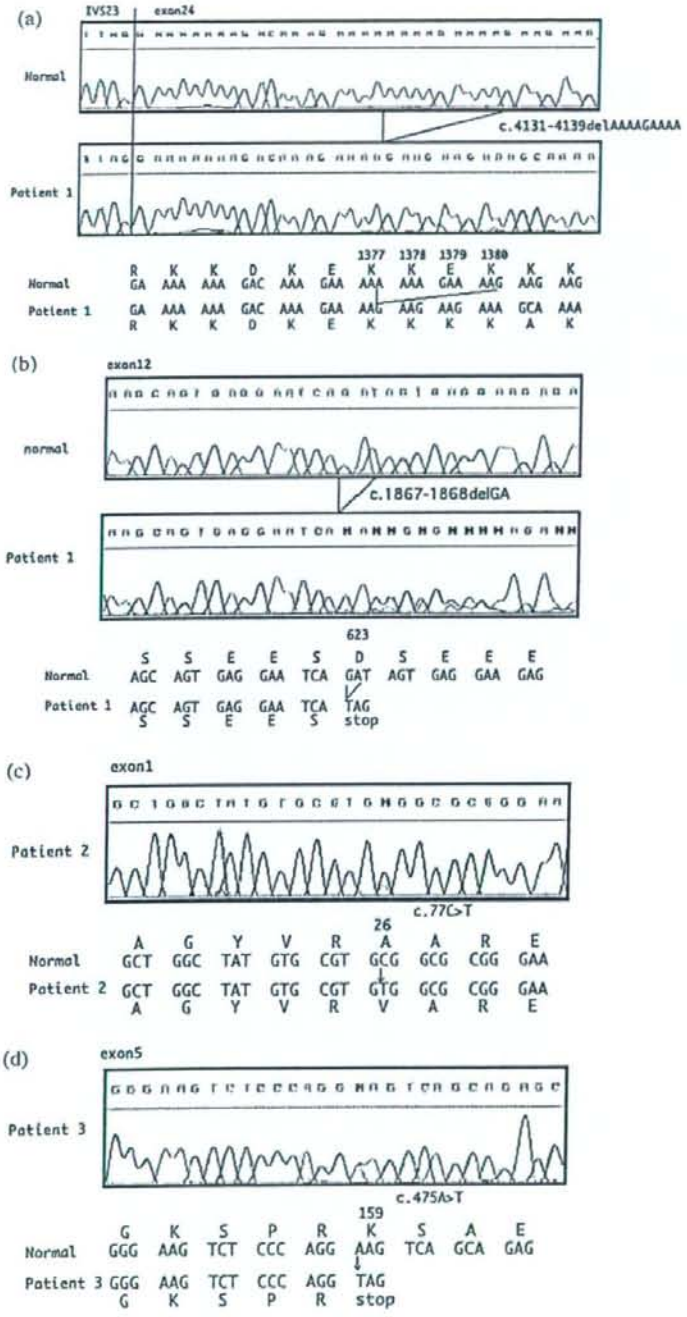

Fig. 1 *TCOF1* mutational analysis for patients 1, 2 and 3. (a) Sequence of a part of exon 24 from a normal individual and patient 1's mutant allele. The results for patient 1 were obtained after TA cloning. It was found that patient 1 had the heterozygous deletion (c.4131-4139delAAAAGAAAA) in his mutant allele. Predicted amino acid sequences of a normal individual and patient 1 are also shown. In patient 1, three amino acids (K-E-K) would be deleted from the treacle amino acid sequence. (b) Sequence of a part of exon 12 from a normal individual and patient 1 (genomic polymerase chain reaction [PCR] sequence). Patient 1 has a 2 bp deletion, which is expected to result in frameshift and a premature stop codon (p.D623X). (c) Patient 2 has a missense mutation (c.77C>T; genomic PCR sequence). Predicted amino acid sequences of a normal individual and patient 2 are shown. c.77C>T would cause the substitution (p.A26V). (d) Patient 3 has a single base substitution (c.475A>T), resulting in a nonsense mutation (p.K159X) and truncation of the treacle protein (genomic PCR sequence).

References

1 Dixon J, Edwards SJ, Anderson I *et al.* Identification of the complete coding sequence and genomic organization of the Treacher Collins syndrome gene. *Genome Res.* 1997; **7**: 223–4.

2 Wise CA, Chiang LC, Paznekas WA *et al.* TCOF1 gene encodes a putative nucleolar phosphoprotein that exhibits mutations in Treacher Collins Syndrome throughout its coding region. *Proc. Natl Acad. Sci. USA* 1997; **94**: 3110–15.

3 Marsh KL, Dixon J, Dixon MJ. Mutations in the Treacher Collins syndrome gene lead to mislocalization of the nucleolar protein treacle. *Hum. Mol. Genet.* 1998; **7**: 1795–800.

4 Winokur ST, Shiang R. The Treacher Collins syndrome (TCOF1) gene product, treacle, is targeted to the nucleolus by signals in its C-terminus. *Hum. Mol. Genet.* 1998; **7**: 1947–52.

5 Valdez BC, Henning D, So RB, Dixon J, Dixon MJ. The Treacher Collins syndrome (TCOF1) gene product is involved in ribosomal DNA gene transcription by interacting with upstream binding factor. *Proc. Natl Acad. Sci. USA* 2004; **101**: 10 709–14.

6 Dixon J, Jones NC, Sandell LL *et al.* Tcof1/Treacle is required for neural crest cell formation and proliferation deficiencies that cause craniofacial abnormalities. *Proc. Natl Acad. Sci. USA* 2006; **103**: 13 403–8.

7 Edwards SJ, Gladwin AJ, Dixon MJ. The mutational spectrum in Treacher Collins syndrome reveals a predominance of mutations that create a premature-termination codon. *Am. J. Hum. Genet.* 1997; **60**: 515–24.

8 Horiuchi K, Ariga T, Fujioka H *et al.* Mutational analysis of the TCOF1 gene in 11 Japanese patients with Teacher Collins syndrome and mechanism of mutagenesis. *Am. J. Med. Genet.* 2005; **134A**: 363–7.

9 Splendore A, Silva EO, Alonso LG *et al.* High mutation detection rate in TCOF1 among Treacher Collins syndrome patients reveals clustering of mutations and 16 novel pathogenic changes. *Hum. Mutat.* 2000; **16**: 315–22.

10 Dixon J, Hovanes K, Shiang R, Dixon MJ. Sequence analysis, identification of evolutionary conserved motifs and expression analysis of murine tcof1 provide further evidence for a potential function for the gene and its human homologue, TCOF1. *Hum. Mol. Genet.* 1997; **6**: 727–37.

11 Splendore A, Fanganiello RD, Masotti C, Morganti LS, Passos-Bueno MR. TCOF1 mutation database: Novel mutation in the alternatively spliced exon 6A and update in mutation nomenclature. *Hum. Mutat.* 2005; **25**: 429–34.

12 Ellis PE, Dawson M, Dixon MJ. Mutation testing in Treacher Collins Syndrome. *J. Orthod.* 2002; **29**: 293–7.

13 Splendore A, Jabs EW, Passos-Bueno MR. Screening of TCOF1 in patients from different populations: Confirmation of mutational hot spots and identification of a novel missense mutation that suggests an important functional domain in the protein treacle. *J. Med. Genet.* 2002; **39**: 493–5.

14 Gerlitz G, Darhin E, Giorgio G, Franco B, Reiner O. Novel functional features of the Lis-H domain: Role in protein dimerization, half-life and cellular localization. *Cell Cycle* 2005; **4**: 1632–40.

15 Emes RD, Ponting CP. A new sequence motif linking lissencephaly, Treacher Collins and oral-facial-digital type 1 syndromes, microtubule dynamics and cell migration. *Hum. Mol. Genet.* 2001; **10**: 2813–20.

16 Kim MH, Cooper DR, Oleksy A *et al.* The structure of the N-terminal domain of the product of the lissencephaly gene Lis1 and its functional implications. *Structure* 2004; **12**: 987–98.

Journal of Plastic, Reconstructive & Aesthetic Surgery (2008) 61, 257–264

ELSEVIER

JPRAS
An International Journal of Surgical Reconstruction
www.JPRASurg.com

Double innervation occurs in the facial mimetic muscles after facial-hypoglossal end-to-side neural repair: rat model for neural supercharge concept

Hiroshi Furukawa*, Akira Saito, William Mol, Mitsuru Sekido, Satoru Sasaki, Yuhei Yamamoto

Department of Plastic and Reconstructive Surgery, Graduate School of Medicine, University of Hokkaido at Sapporo (UHS), Kita-15 Nishi-7, Kita-Ku, Sapporo, Hokkaido 060-8638, Japan

Received 3 September 2006; accepted 22 January 2007

KEYWORDS
Double innervation;
Facial mimetic muscles;
Neural supercharge concept;
End-to-side neurorrhaphy;
Synkinesis;
Persistent incomplete facial palsy

Summary *Background:* Double innervation of facial mimetic muscles by both facial and hypoglossal nerves after end-to-side neurorrhaphy has not been proven, although facial —hypoglossal end-to-side neurorrhaphy has been used in persistent incomplete facial palsy recently, and has achieved clinical evidences of recovery with rare synkinesis. We established a rat model to compare synkinesis after end-to-end and end-to-side neurorrhaphy techniques between facial and hypoglossal nerves, and confirmed double innervation using retrograde tracers.

Methods: Rats were divided into three groups (each consisting of six rats), a facial palsy group (Group A), a facial-hypoglossal end-to-end neurorrhaphy group (Group B), and a facial-hypoglossal end-to-side neurorrhaphy group (Group C). Eight weeks after surgery, synkinesis of the facial mimetic muscles was observed and recorded via video camera. In Group C, post operative, intramuscular injections of retrograde neural tracers (Fast Blue, Diamidino Yellow and DiI) into the facial mimetic muscles were performed to prove double innnervation by both the facial and hypoglossal nerves.

Results: In Group B, all rats showed facial palsy. However while eating and drinking, their half of the face showed mass movements (strong contraction of whisker pad muscles, curved nose and eye-closure). In Group C, four rats showed no significant changes however, two rats showed synkinesis of the eyelid while eating and drinking (frequent eye-closure distinguishable from the contralateral normal side). In Group C, retrograde tracers injected in the mimetic muscles were detected in both the facial and hypoglossal motor nuclei in situ of all the rats' brain stem.

Conclusion: This study proved that double innervation of mimetic muscles by both facial and hypoglossal nerves occurs after the end-to-side neurorrhaphy. Double-innervated mimetic

* Corresponding author. Address: Department of Plastic and Reconstructive Surgery, Graduate School of Medicine, University of Hokkaido at Sapporo (UHS), Kita-15 Nishi-7, Kita-Ku, Sapporo, Hokkaido 060-8638, Japan. Tel.: +81 11 716 1161x6978; fax: +81 11 706 7827.
E-mail address: hfuru@med.hokudai.ac.jp (H. Furukawa).

1748-6815/$ - see front matter
doi:10.1016/j.bjps.2007.01.075

muscles around the mouth after hypoglossal-facial end-to-side neurorrhaphy showed less synkinesis than the end-to-end neurorrhaphy.

The hypoglossal-facial nerve neurorrhaphy technique is the popular surgical procedure to re-innervate facial mimetic muscles after injury of the facial nerve,[1,2] especially done after complete facial palsy. For the treatment of persistent incomplete facial palsy, we presented the alternative technique of facial nerve rehabilitation surgery based on double innervation of the paralysed mimetic muscle supplied by both facial and hypoglossal motor nerves recently.[3,4] In order to create a 'neural network' between these two motor neurons, and to preserve remaining facial nerve function, neural communication is created using the end-to-side neurorrhaphy technique. To achieve this, an interpositional nerve graft is placed between the hypoglossal nerve and the facial nerve, and anastomosed with the lateral aspects of both nerves by an end-to-side fashion. The purpose of such a procedure is to preserve and augment the remaining function of facial nerve function after incomplete facial palsy. The end-to-side neurorrhaphy technique may induce double innervation of mimetic muscles by two different motor nerves, the facial and hypoglossal nerves.

The desirable clinical outcome in association with the rare synkinesis has been observed in our clinical series.[3,4] However, anatomical evidence of double innervated mimetic muscles has not been fully elucidated. Although, from clinical observations, it could be postulated that both facial and hypoglossal nerves are innervated into mimetic muscles, it is practically difficult to confirm double innervation at the axonal and nuclei level in clinical cases. Synkinesis is a rare occurrence in some clinical cases and its mechanism remains unclear.

This article reports a rat model for which the end-to-side neurorrhaphy technique between the lateral aspect of the facial nerve and the proximal blunt end of hypoglossal nerve was performed. The purpose of this study is to analyse whether double innervation into mimetic muscles occurs or not after end-to-side neurorrhaphy technique between facial and hypoglossal nerves, and to compare the synkinesis between end-to-end and end-to-side neurorrhaphy technique using a video camera. We have also analysed the state of innervation at facial mimetic muscles after the end-to-side neurorrhaphy using the standard method of post-operative intramuscular injections of widely used retrograde neural tracers.

Materials and methods

Animals

Eighteen adult Wistar male rats (300–350 g) were used for this study. Before and after the experiments, all rats were kept on standard laboratory food and water with an artificial light–dark cycle of 12 h on, 12 h off. All experiments were conducted under anaesthesia in accordance with Guidelines for the Care and Use of Laboratory Animals in the Hokkaido University School of Medicine. All procedure used in this study were approved by the local committee (Animal Care and Use Committee, Hokkaido University School of Medicine).

Experimental groups

The rats were randomly divided into three groups of six rats. Six rats served as the facial palsy group (Group A), six rats as the end-to-end facial-hypoglossal neurorrhaphy group (Group B), and the other six underwent end-to-side facial-hypoglossal neurorrhaphy (Group C) (Fig. 1). In all rats, transection and repair of nerves were carried out on the left side under an operating microscope. Following intraperitoneal injection of Pentobarbital sodium at 30 mg per kg body weight, the trunk of the left facial nerve was exposed in all rats (Fig. 2(a)). In Group A and B, the left facial nerve was transected close to its emergence from the stylomastoid foramen, but distal to the posterior auricular nerve. The proximal stump of facial nerve was diathermied, turned over, and buried in muscle in order to avoid re-innervation without neural repair. In Group B and C, the left hypoglossal nerve was exposed and transected under the oral floor. In Group B, the proximal stump of the hypoglossal nerve was then microsurgically anastomosed to the distal stump of facial nerve with the end-to-end fashion using 11-0 epineural sutures (Ethicon EH 7438G; Norderstedt, Germany). In Group C, the proximal stump of the hypoglossal nerve was then microsurgically repaired to the lateral aspect of the facial nerve with the end-to-side, epineural window technique. The epineural window was created by the removal of the epineural sheath at the main trunk of the facial nerve site. The epineurium of the stamp of hypoglossal nerve was then fixed to the edge of epineural window at facial nerve by six interrupted sutures. In order to preserve facial nerve function, partial neurectomy of the facial nerve at the end-to-side neurorrhaphy was not applied. Finally the wound was closed by 6-0 nylon (Fig. 2(b)).

Video recording of synkinesis

Eight weeks after surgery, the presence of synkinesis of mimetic muscles was checked for and recorded with a video camera. We took more than three sequences in each rat. We used software, QuickTime version 7, for managing video data. The evaluation point was mass movements including whisker pad and/or eyelid during the eating and drinking.

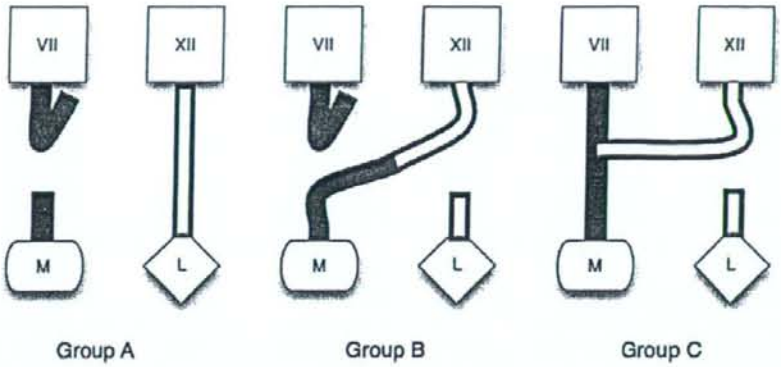

Figure 1 Schematic illustration of each group of the animal models. (VII, facial nuclei; XII, hypoglossal nuclei; M, facial mimetic muscles; L, muscle linguae; black line, facial nerve; white line, hypoglossal nerve.)

Neural tracers

The tracer Fast Blue (FB) and Diamidino Yellow (DY) from SIGMA-ALDRICH (Steinheim, Germany) and DiI (1,1′-dioctadecyl-3,3,3′,3′-tetramethylindocarbocyanin perchlorat) from Molecular Probes (Leiden, The Netherlands) were used for retro-grade neural tracing in our study. FB and DY (FB–DY) were injected into the same muscle simultaneously in order to enhance the detection of the trace within the neural cells. FB stains the cytosol, while DY stains the nuclei of neural cells.

Postoperative retrograde labelling

Eight weeks after surgery, the operated rats received 100 μl of 1% solution of DiI and/or 100 μl of 1% solution of Fast Blue (FB) and/or 200 μl of 0.2% solution of Diamidino Yellow (DY) into the left mimetic muscles (whisker pads and/or upper eyelid) under light diethylether anaesthesia. In principle, FB–DY was injected in whisker pad (whisker pad muscle), and DiI was injected in the upper eyelid (orbicularis oculi muscle). In one rat in Group C, both FB–DY and DiI were injected in whisker pad muscle in order to confirm that double innervation can be detected by both retro grade tracers in the same way (the variety of tracer does not effect the detection of double innervation). Two weeks after the tracer injection, those rats were sacrificed and were perfused by 4% paraformaldehyde as explained below. Pre-experimental trials confirmed the optimum detection of the tracers, following this timing and conditions.

Fixation and tissue processing

Firstly, the rats were lightly anaesthetised using diethylether followed by 30 mg per kg body weight of Pentobarbital sodium, injected intraperitoneally. Secondly, all rats of groups B and C were transcardially perfused with 0.9% NaCl followed by a fixation with 4% paraformaldehyde in a 0.1 M phosphate buffer, pH 7.4 for 20 min. Thirdly, the brains were removed and 50 μm-thick coronal sections were cut through the brainstems using a cryotome, LEICA CM1900. The specimens were studied using an Olympus Provis

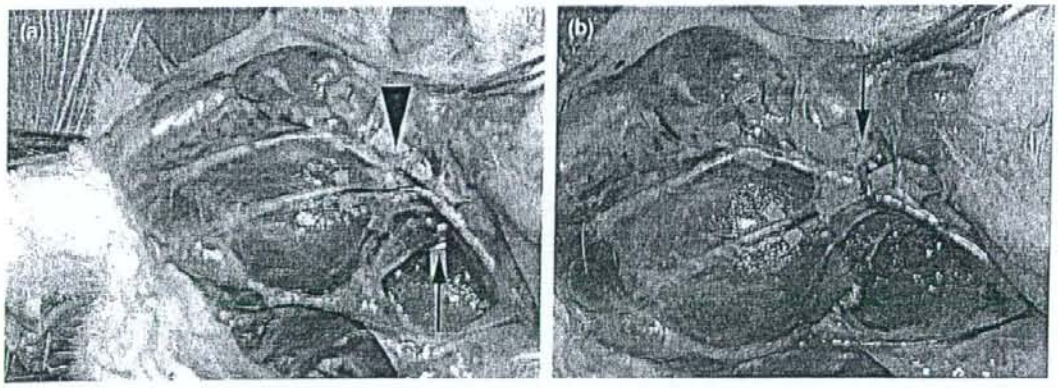

Figure 2 End-to-side neurorrhaphy between facial and hypoglossal nerves in Group C. (a) Dissection of facial nerve trunk (arrowhead) and hypoglossal nerve (arrow) in the rat. (b) View after end-to-side neurorrhaphy (arrow).

AX-70 microscope equipped with a range of objective lenses (4X, 10X and 20X). Sections were observed through an UV-excitation filter (WU), which allows recognition of FB-labelled neurons (blue), DY-labelled nuclei (white), and rhodamine-filter (WIG), which allows recognition of DiI-labelled neuron (Texas red or yellow). Two separate images from the same field were captured with two different filters corresponding to the specific combination of the tracers. The images were captured directly with an Olympus DP 70 and were processed with an Olympus DP Controller (all from Olympus Optical, Tokyo), which converted and exported images in a tagged-image file format (TIFF).

Results

Synkinesis

In Group A, all six rats showed left facial palsy (loss of blink reflex by a puff of air to the cornea, loss of whisker movements; data not shown). In Group B, hemifacial mass contraction was observed in all six rats (Fig. 3). They displayed facial palsy, but when eating and drinking, the left half of their faces (ipsilateral side) showed mass movements (strong contraction of whisker pad muscles, curved nose and eye-closure). In Group C, four of the six rats presented no special changes except for tongue atrophy (we defined this subset as Group C-1). However, two of the six rats presented synkinesis of the left (ipsilateral) eyelid while eating and drinking (frequent eye-closure distinguishable from the contralateral normal side). This subset is defined as Group C-2.

Tracer study

In Group B, all rats, both FB—DY and DiI-labelled nuclei were recognised in the left hypoglossal nuclei, following the injection of FB—DY into the whisker pad muscle, and DiI into the orbicularis oculi muscle (Fig. 4), but not recognised in the facial nuclei (data not shown). In Group B, the left facial nerves were anastomosed with the hypoglossal nerves using the end-to-end neurorrhaphy technique. Therefore, tracer-labelled hypoglossal nuclei signify that left mimetic muscles were innervated by hypoglossal nuclei, instead of the facial nuclei. In Group C, FB—DY double-labelled nuclei were detected in both left hypoglossal nuclei and left facial nuclei regions, in all rats, following the injection FB—DY into their whisker pad muscles. In one rat of Group C, both FB—DY double-labelled and DiI-labelled nuclei were detected in both left hypoglossal and facial nuclei regions, following the injection of both FB—DY and DiI into the whisker pad muscle (Fig. 5). In Group C, the left hypoglossal nerves were joined with the left facial nerves using the end-to-side neurorrhaphy technique. This result proves that the left facial mimetic muscles were innervated by both the left facial and left hypoglossal nerve nuclei. In Group C-1, FB—DY injected into the whisker pad muscle was detected in hypoglossal nerve nuclei (Fig. 6(a)). However, the DiI, that was injected into the upper eyelid was not detected in any sections of hypoglossal nerve nuclei region of the brain stem (Fig. 6(b)). In Group C-2, both FB—DY injected into the whisker pad muscles and DiI injected into the upper eyelid were detected in the hypoglossal nerve nuclei (Fig. 6(c) and (d)).

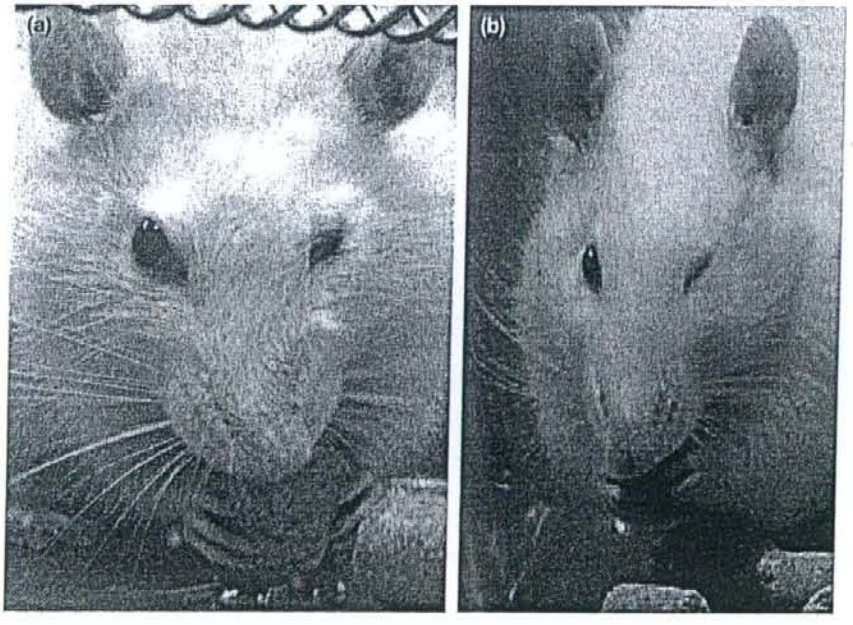

Figure 3 (a) Appearance of the face in Group B rat, 2 months postoperative, at eating. (b) Appearance of the face in Group C-2 rat, 2 months postoperative, at eating.

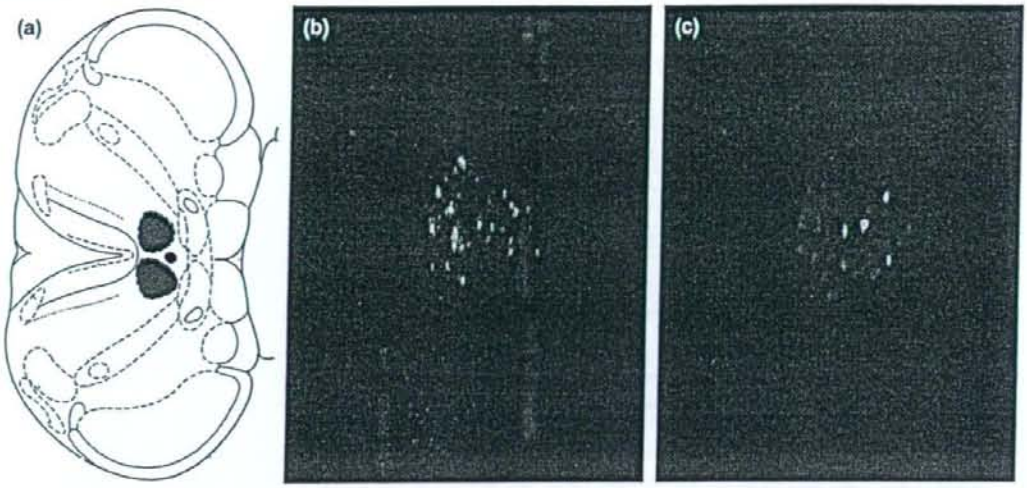

Figure 4 Photomicrographs of transverse sections through the hypoglossal nuclei in Group B showing labelled motoneurons after injection of FB—DY to the left whisker pad muscle and DiI to the left orbicularis oculi muscle. Two separate images from the same field were captured with two different filters corresponding to the specific combination of the tracers. (a) Horizontal diagram of the rat brain stem at the level of Medulla Oblongata. Red area indicates hypoglossal nuclei. Adapted from *The Rat Brain in Stereotaxic Coordinates, Fourth Edition, George Paxinos and Charles Watson, Academic Press, Sandiego, 1998.*[9] (b) Labelling in the left side of hypoglossal nuclei through UV-filter following FB—DY application to whisker pad muscle (20×). (c) The same field through rhodamine-filter. Labelling in hypoglossal nuclei following DiI application to orbicularis oculi muscle (20×).

Discussion

For the treatment of persistent incomplete facial palsy, we presented the alternative technique of facial nerve rehabilitation surgery based on double innervation of the paralysed mimetic muscle supplied by both facial and hypoglossal motor nerves recently.[3,4] The reason why we established double-innervated mimetic muscle model of rat is that we would like to prove double innervated mimetic muscle by the end-to-side neurorrhaphy technique using retrograde tracer. It is difficult to confirm double innervation at the axonal and nuclei level in clinical cases. We also need to confirm the hypothesis 'end-to-side neurorrhaphy present less synkinesis'. The synkinesis by double innervation can be evaluated by videorecording of the rat. Our model allows us to activate the hypoglossal nerve by feeding the rat.

Our Group C rat is not incomplete facial palsy model, such like controlled crush of the facial nerve. Because our first priority is proof of double innervation by the end-to-side neurorrhaphy technique, rather than establishment of an incomplete facial palsy model, we used intact facial nerve in Group C. Although we have no data for quantification with the regenerating axons passing the end-to-side window, we guess epineural window technique may allow much more sprouting compared with no window technique. If the hypothesis 'end-to-side anastomosis present less synkinesis' is correct, much more sprouting is much better in the clinical reconstructive cases, so we performed epineural window technique in Group C.

In this study, at first, we presented that double-innervation is inducible at the axon level by the end-to-side neurorrhaphy technique. We used FB, DY and DiI, and all agents worked successfully as retro grade neural tracers. Labelled nuclei were detected on left facial nuclei and hypoglossal nuclei in all rats after end-to-side neurorrhaphy technique. This means facial nerve was 'supercharged' or 'augumented' by the hypoglossal nerve, although the facial nerve in type C was normal and not facial palsy model at our study.

Surgical creation of new neural networks using the end-to-side neurorrhaphy can give rise to synkinesis. However, the occurrence of synkinesis is rare in our clinical cases. Such a desirable clinical outcome with rare synkinesis is supported by an unknown mechanism. One of the reasons for the delayed study in this field is the lack of a reproducible experimental approach allowing an unbiased comparison of synkinesis between the pre- and post-surgical innervation, and between end-to-side and end-to-end neurorrhaphy in animal study. Because our end-to-side double-innervated model is focused on the relationship between intact facial nerve and hypoglossal nerve, it is easier to evaluate synkinesis than other pairs of neurons. When rats eat or drink, synkinesis of mimetic muscles can be recorded and evaluated via video camera. In fact, two months after end-to-end neurorrhaphy between facial and hypoglossal nerves, all rats showed synkinesis while eating and drinking. Their mimetic muscles in the operative site in Group B presented mass movements and their eyes tightly closed.

Conversely, our experiments showed that the end-to-side double-innervated group (Group C) did not show synkinesis except for eyelid movements in a few rats (Group C-2). Why did the end-to-side double-innervated group not show synkinesis like the mass movements shown by the end-to-end group? How can we explain the discrepancy between

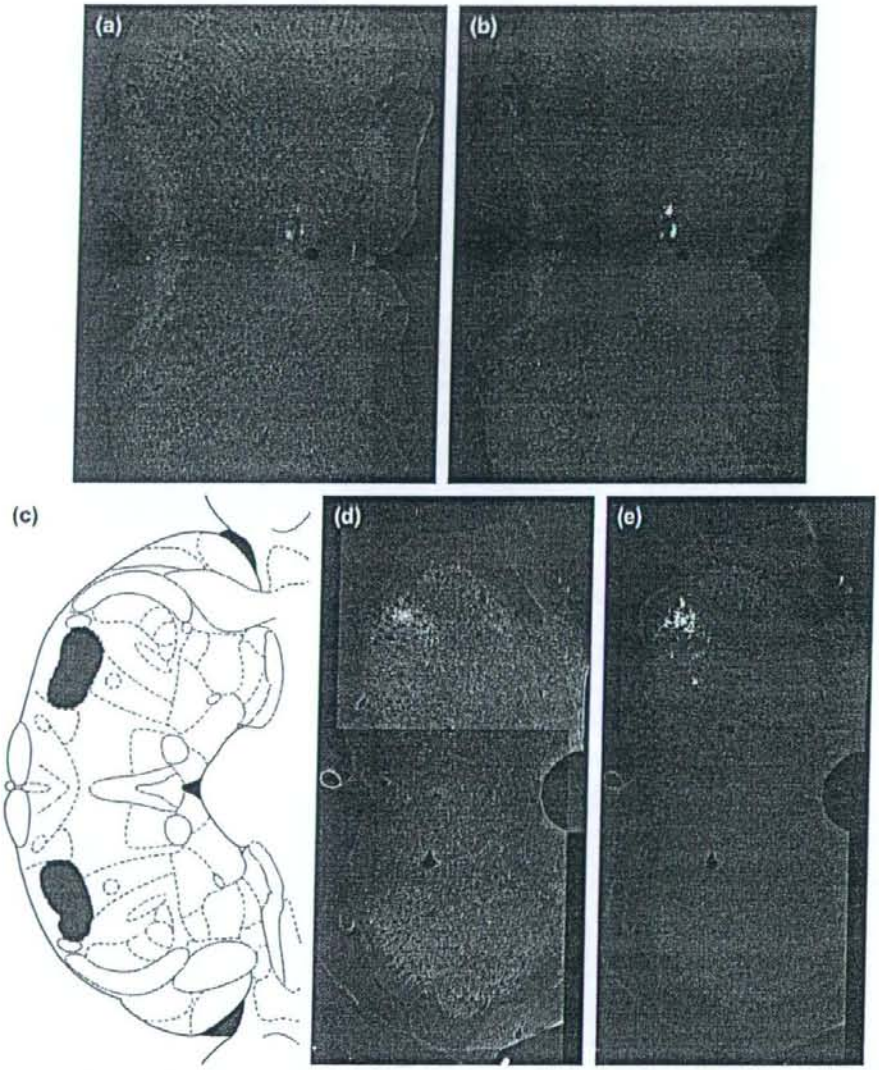

Figure 5 Results of FB–DY and DiI injections into the left whisker pad muscle in Group C. (a) Labelling in the left side of hypoglossal nuclei following application FB–DY to whisker pad muscle (10×). (b) The same field through rhodamine-filter. Labelling in the left side of hypoglossal nuclei following DiI application to whisker pad muscle (10×). (c) Horizontal diagram of the rat brain stem at the level of Pons. Red area indicates facial nuclei. Adapted from the same reference[9] of Fig. 4. (d) FB–DY labelled facial nuclei in the same rat (10×). (e) DiI-labelled facial nuclei in the same field under rhodamine-filter (10×).

the result of tracer study (double innervated whisker pad muscle) and video study (no synkinesis around whisker pad)?

There is one possibility that the ratio of the innervation between facial and hypoglossal nerves decides the phenotype of synkinesis. Setting the innervation ratio between facial and hypoglossal nerves is impossible by our surgical procedure, so we tried to approach this question by dennervation of facial nerve after end-to-side neurorrhaphy. Eight weeks after end-to-side neurorrhaphy, we cut the facial nerve trunk at the proximal side of the anastomosed site. Just after cutting the facial nerve, rat presented the phenotype of facial palsy. Rats started to show the same synkinesis as with the end-to-end group, at 2–4 weeks later (data is not shown). This suggests that hypoglossal neurons, which innervate in mimetic muscle through end-to-side T-portion, did not cause synkinesis even when the innervation ratio is converted to 100%. Instead, the absolute amount of axons derived from hypoglossal nerve may be

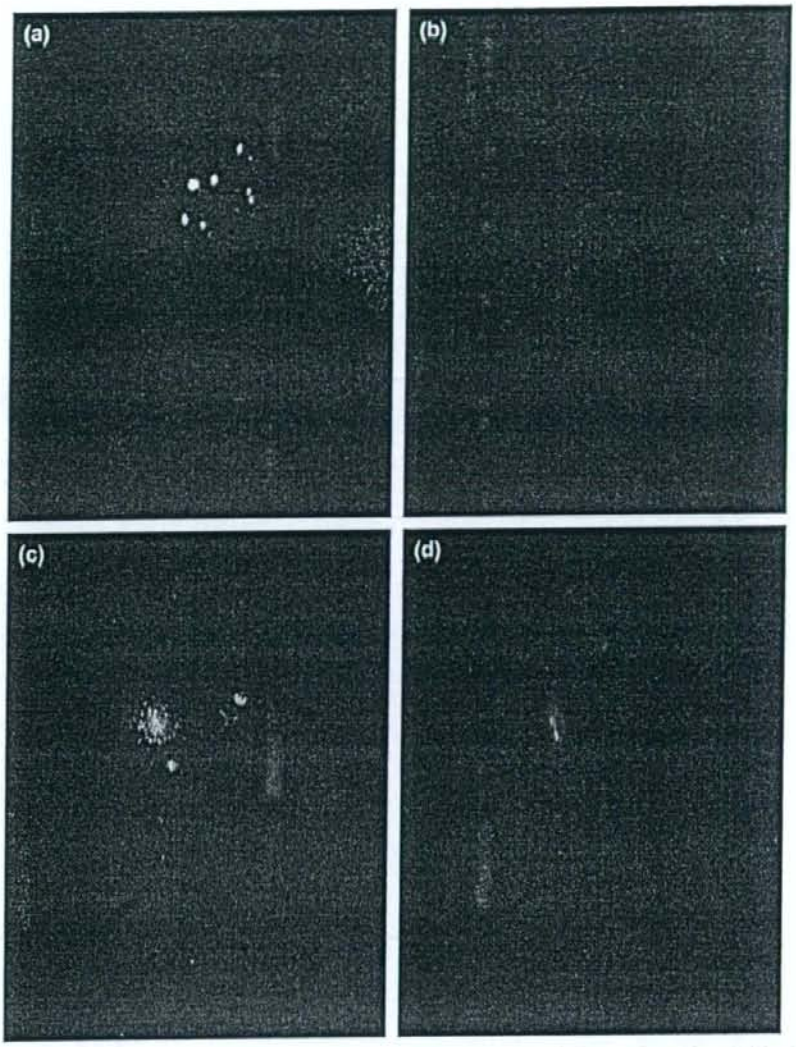

Figure 6 Labelled hypoglossal nuclei in Group C, following FB–DY application to whisker pad muscle and DiI application to orbicularis oculi muscle. (a) Labelled hypoglossal nuclei in Group C-1 through UV-filter (20×). (b) Photo of the same field under rhodamine-filter (20×). (c) Labelled hypoglossal nuclei in Group C-2, under UV-filter (20×). (d) Photo of the same section in Group C-2, under rhodamine-filter (20×).

the important factor of synkinesis. In Group C, the axons of the hypoglossal nerve may grow into the sheath of the facial nerve, and if there is a lesion on facial nerve, the axons of the hypoglossal nerve may replace axons of the facial nerve. This extra data also suggests that intact facial neurons might inhibit the sprouting of hypoglossal nerve at the T-portion, and some neural blunt ends of hypoglossal nerve are waiting for the chance of innervation until facial nerve is dennervated.

There is another possibility for the reason why synkinesis was rare in the end-to-side double-innervated group except for the eyelid. At the level of the brain stem of intact rats, the hypoglossal neurons project axons to the facial nucleus and neurons of the parvocellular reticular nucleus innervate facial and hypoglossal motoneurons simultaneously. All these connections should represent the anatomical explanation for coordination of movements of the tongue and face during several activities like swallowing and vocalisation.[5,6] Popratiloff AS et al. recently reported hypoglossal and reticular interneurons involved in oro-facial coordination in the rats.[7] Such interneurons in rat brain stem coordinating both digestion and eyelid movement has not been reported.

Putting them together, we suppose that shared innervation of both facial and hypoglossal nuclei in the brain stem may prevent synkinesis of the doubly innervated mimetic muscles around the mouth. We hypothesize that other pairs of two motor nerves, of which nuclei were anatomically or accidentally shared-innervated in the brain stem or in spinal cord, can also be made into a network without harmful synkinesis. Rubin LR et al. commented on 'Dr. Rosene's pathway' between the facial nerve and trigeminal nerve long after reanimation surgery using temporalis and masseter muscles.[8] Trigeminal nucleus may sprout, with the fifth nerve neurons taking over the seventh nerve nucleus. The impulse to smile passed on to both seventh and fifth cranial nuclei, but concentrated on the relocated muscles, because of injured facial nerve.[8] In the future, study focused on pre-existence of connections in central nerve system will solve this hypothesis, and select the candidate of the combination of nerves for useful network-like reconstruction.

Acknowledgement

The authors wish to acknowledge Prof. Masahiko Watanabe M.D., Ph.D., Department of Anatomy, Hokkaido University Graduate School of Medicine for great help in completing this study. This work was supported by a Grant-in-Aid for Exploratory Research from the Japanese Ministry of Education, Culture, Sports, Science, and Technology (18659523).

References

1. May M, Sobol SM, Mester SJ. Hypoglossal-facial nerve interpositional-jump graft for facial reanimation without tongue atrophy. *Otolaryngol Head Neck Surg* 1991;104:818–25.
2. Yoleri L, Songur E, Yoleri O, et al. Reanimation of early facial paralysis with hypoglossal/facial end-to-side neurorrhaphy: a new approach. *J Reconstr Microsurg* 2000;16:347–55 [discussion 55–6].
3. Yamamoto Y, Sasaki S, Sekido M, et al. Alternative approach using the combined technique of nerve crossover and cross-nerve grafting for reanimation of facial palsy. *Microsurgery* 2003;23:251–6.
4. Yamamoto Y, Sekido M, Furukawa H, et al. Surgical rehabilitation of reversible facial palsy: facial-hypoglossal network system based on neural signal augumentation/neural supercharge concept. *JPRAS* 2007;60:223–31.
5. Fernandez E, Lauretti L, Denaro L, et al. Motoneurons innervating facial muscles after hypoglossal and hemihypoglossal-facial nerve anastomosis in rats. *Neurol Res* 2004;26:395–400.
6. Streppel M, Popratiloff A, Gruart A, et al. Morphological connections between the Hypoglassal and facial nerve in the brain stem of the rat. *HNO* 2000;48:911–6.
7. Popratiloff AS, Streppel M, Gruart A, et al. Hypoglossal and reticular interneurons involved in oro-facial coordination in the rat. *J Comp Neurol* 2001;433:364–79.
8. Rubin LR, Rubin JP, Simpson RL, et al. The search for the neurocranial pathways to the fifth nerve nucleus in the reanimation of the paralyzed face. *Plast Reconstr Surg* 1999;103:1725–8.
9. George Paxinos CW. *The rat brain in stereotaxic coordinates*. 4th ed. Sandiego: Academic Press Harcourt Brace & Company; 1998.

PAX4 has the potential to function as a tumor suppressor in human melanoma

SHINYA HATA[1,2], JUN-ICHI HAMADA[1], KAZUHIKO MAEDA[1,2], TAICHI MURAI[1], MITSUHIRO TADA[1], HIROSHI FURUKAWA[2], ARATA TSUTSUMIDA[2], AKIRA SAITO[2], YUHEI YAMAMOTO[2] and TETSUYA MORIUCHI[1]

[1]Division of Cancer-Related Genes, Institute for Genetic Medicine, Hokkaido University, Kita-15, Nishi-7, Kita-ku, Sapporo 060-0815; [2]Department of Plastic and Reconstructive Surgery, Graduate School of Medicine, Hokkaido University, Kita-15, Nishi-7, Kita-ku, Sapporo 060-8638, Japan

Received May 29, 2008; Accepted July 22, 2008

DOI: 10.3892/ijo_00000095

Abstract. We hypothesize that dysregulated expression levels of the developmental regulatory genes in the adult body result in tumor development and malignant progression. *PAX* genes discovered as human orthologous genes of *Drosophila 'paired'* encode transcription factors, which control the expression of target genes to go on along the program of development. In this study, we first quantified expression of 9 *PAX* genes in human nevus pigmentosus tissues, melanoma tissues and melanoma cell lines by the real-time reverse transcription-PCR method. As a result, we found that the expression levels of *PAX4* and *PAX9* were extremely low in melanoma tissues and cell lines compared to nevus pigmentosus tissues. We then established melanoma cells overexpressing *PAX4* and examined roles of *PAX4* in cell growth. *PAX4*-overexpression reduced *in vitro* cell growth of human melanoma C8161 and MeWo cells. BrdU-uptake assay and cell cycle analysis by flow cytometry indicated that the retardation of cell proliferation by *PAX4*-overexpression was due to decreased DNA synthesis and cell cycle arrest at the G0/G1 phase. Furthermore, treatment of C8161 and MeWo cells with 5-azacytidine, a DNA demethylating agent, induced the expression of *PAX4*, suggesting that DNA methylation repressed the *PAX4* gene expression in human melanoma. These results suggest that PAX4 functions as a potent tumor suppressor.

Correspondence to: Dr Jun-ichi Hamada, Division of Cancer-Related Genes, Institute for Genetic Medicine, Hokkaido University, Kita-15, Nishi-7, Kita-ku, Sapporo 060-0815, Japan
E-mail: jhamada@igm.hokudai.ac.jp

Key words: PAX4, melanoma, tumor suppressor

Introduction

The development of cancer and its malignant progression can be considered as a phenomenon where cancer cells go on along a part of the program of embryogenesis. The genes regulating embryonic development spatio-temporally express themselves in an exquisitely controlled manner and execute programs such as cell growth, migration, differentiation and death. It is thought that abnormal cell behaviour of tumor cells result from the mis-execution of such a program.

PAX genes, one of the developmental regulatory genes, were discovered as a human orthologous gene of *Drosophila 'paired'* (1). In human, 9 *PAX* genes have been identified (2,3). All *PAX* genes commonly possess a paired box, which consists of 381 bp. The paired box encodes paired domain through which PAX proteins bind to DNA in a sequence-specific manner in order to function as transcription factors.

It is known that abnormal expression of *PAX* genes causes various types of congenital abnormality. For example, mutations of *Pax1* and *Pax3* show the developmental defect of centrum and intervertebral disc and Splotch in mice, respectively (4,5). The mutation of *PAX2* and *PAX6* causes optic nerve colobomas, renal anomalies and congenital eye abnormalities including aniridia, respectively (6,7).

There are also some studies indicating that abnormal expression of *PAX* genes is associated with cancer development and behaviour. Abnormal expression levels of *PAX* genes through chromosomal translocations are found in rhabdomyosarcoma, thyroid cancer and acute lymphoblastic leukemia (8-11). Constitutive expression of *PAX2*, *PAX3*, *PAX5* or *PAX6* was detected in Ewing sarcoma, Wilms' tumor, medulloblastoma or thyroid cancer (12-15). Forced expression of *Pax1*, *Pax2*, *Pax3*, *Pax6* or *Pax8* transforms mouse fibroblasts (16). Some studies show that human *PAX2* or *PAX3* plays an essential role in survival of bladder and ovarian cancer cells or melanoma cells (17,18). PAX proteins are also known to alter the expression of tumor suppressor genes: PAX2 and PAX3 regulate the expression of *WT1* and PAX2, PAX5 and PAX8 repress the expression of p53 (19-21). Thus

dysregulated expression of a particular *PAX* gene(s) is likely to be involved in carcinogenesis and the malignant progression of a variety of cancers.

To explore malignant behaviour-associated *PAX* genes, we established an analysis system to quantify the expression of 9 human *PAX* genes at the level of mRNA. Using this system, we first compared the expression levels of 9 *PAX* genes between malignant melanoma specimens and nevus pigmentosus specimens. Furthermore, we addressed the tumor-suppressive role of *PAX4* of which expression was lost or extremely low in melanoma compared to nevus tissues.

Materials and methods

Clinical specimens. We studied 16 cutaneous melanoma tissues and 5 nevus tissues from patients who had undergone surgery at the Department of Plastic Surgery, Hokkaido University Medical Hospital between 1996 and 2003. The age of the patients ranged from 29 to 87 years and gender breakdown was 6 males and 10 females. The tumor status according to the TNM classification (UICC, 6th edition) was pT1aN0M0 in 3 cases, pT1bN0M0 in 1 case, pT1bN1bM0 in 1 case, pT2aN0M0 in 3 cases, pT3aN1aM0 in 1 case, pT4aN0M0 in 2 cases, pT4bN0M0 in 3 cases, pT4bN1M0 in 1 case and pT4bN2aM0 in 1 case. Complete written informed consent was obtained from all the patients.

Cells and culture condition. Human melanoma C8161 cells were kindly provided by Dr Motowo Nakajima (Johnson and Johnson, Tokyo, Japan). Origin and institution by which other cell lines (MeWo, G361, 9711, GAK, A375M and MMIV) were provided were described in our previous report (22). All the cell lines were grown on tissue culture dishes in a 1: 1 (v/v) mixture of Dulbecco's modified Eagle's minimum essential medium and Ham's F12 medium (DME/F12), supplemented with 10% heat-inactivated fetal bovine serum (FBS, Cambrex Bio Science, Wolkersville, MD). The cells were cultured at 37°C in a CO_2 incubator (5% CO_2 and 95% air).

Transfection and cell cloning. The human *PAX4* expression vector, pCDNA3.1HisA-*PAX4*, was kindly donated by Dr Takahide Miyamoto (Shinshu University School of Medicine) (23). The transfection of pCDNA3.1HisA-PAX4 or pCDNA3.1HisA (Invitrogen, Carlsbad, CA) into MeWo and C8161 cells was performed with Lipofectamine (Invitrogen) and PLUS reagent (Invitrogen) according to the manufacturer's instructions. The cells stably transfected with the pCDNA3.1HisA-PAX4 or pCDNA3.1HisA were selected by their resistance to 100 μg/ml of G418 sulfate (Cellgro, Herndon, VA). Cell cloning of the stable transfectants was performed by picking up the growing colony.

Immunoblot analysis. Melanoma cells cultured on 100-mm dishes were washed with cold PBS and then harvested with a cell scraper in lysis buffer (10 mM Tris-HCl, pH 7.8; 1% NP40; 0.15 M NaCl; 1 mM EDTA; 10 μg/ml of leupeptin, aprotinin and pepstatin A). The cell lysates were centrifuged at 20,000 x g for 30 min at 4°C. The supernatants were collected and the protein concentration was determined by modified Bradford assay (Bio-Rad protein assay, Bio-Rad, Hercules, CA). Equal amounts of protein were separated by SDS-PAGE in 7.5% polyacrylamide gel and electrotransferred to nitrocellulose membranes. After blocking in TBS-T (20 mM Tris-HCl, pH 7.5; 137 mM NaCl; 0.1% Tween-20) containing 5% skim milk, the membranes were incubated with goat anti-human PAX4 antibody (Santa Cruz Biotech., Santa Cruz, CA). The membranes were then incubated with peroxides-conjugated anti-goat IgG antibody (Santa Cruz Biotech.) and developed by reagents from the Enhanced Chemiluminescence Detection System (Amersham Pharmacia Biotech., Piscataway, NJ).

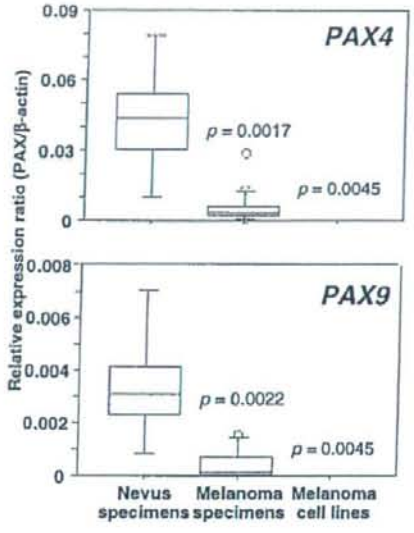

Figure 1. Decreased expression levels of *PAX4* and *PAX9* in melanoma tissues and cell lines. The expression levels of *PAX4* and *PAX9* were quantified by a real-time RT-PCR method. The distribution of the relative expression ratio (*PAX/β-actin*) is shown by using boxplots. The central box in each plot shows the interquartile (25th to 75th percentile) range. The line in the box shows the median. The whiskers (vertical bars) were drawn to the 90th and 10th percentile. Extreme values higher then the 90th percentile or <10th percentile were marked with circles individually. P-values vs. nevus specimens were calculated by the Mann-Whitney U test.

RNA extraction and cDNA preparation. Total RNA was extracted from monolayer cultures of each cell line and clinical specimens by using Trizol (Invitrogen) according to the manufacturer's instructions. Total RNA (1 μg) was subjected to cDNA synthesis in 100 μl of reaction mixture containing Taq Man RT buffer (Applied Biosystems, Foster City, CA), 5.5 mM $MgCl_2$, 500 μM dNTP, 2.5 μM random hexamers, 0.4 U/μl RNAase inhibitor, 1.25 U/μl MultiScribe reverse transcriptase. The reverse transcription reaction was performed sequentially for 10 min at 25°C, for 30 min at 48°C and for 5 min at 95°C.

Quantitative real-time PCR. The PCR primers were designed with the use of Primer Express 1.5 (Applied Biosystems). The primer sequences for amplification of 9 *PAX* genes and ß-actin are listed in Table I. Real-time PCR was carried out with a 15 min hot start at 95°C followed by a denaturation step

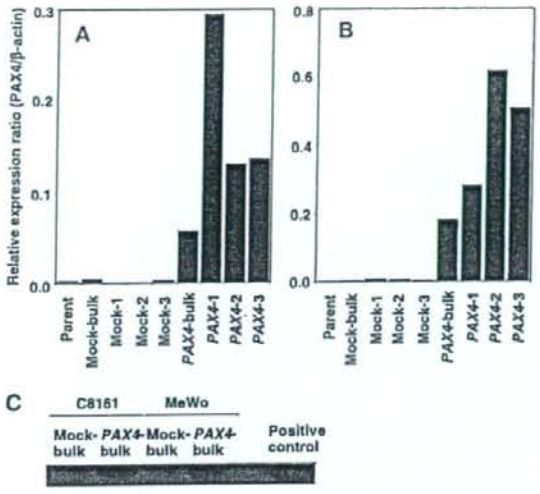

Figure 2. Expression levels of *PAX4* in the melanoma cells transfected with either *PAX4*-expression vectors or the control vectors. Parent, Mock and *PAX4* indicate the cells before the transfection, the cells transfecetd with the control vectors and the cells transfected with the *PAX4* expression vectors, respectively. Mock-bulk and *PAX4*-bulk indicate uncloned cells transfected with either vector. (A and B) Real-time RT-PCR analysis of PAX4 expression in the transfectants from C8161 (A) and MeWo (B). (C) Immunoblot analysis of cell lysates of the cell transfected with the PAX4 expression vectors or the control vectors.

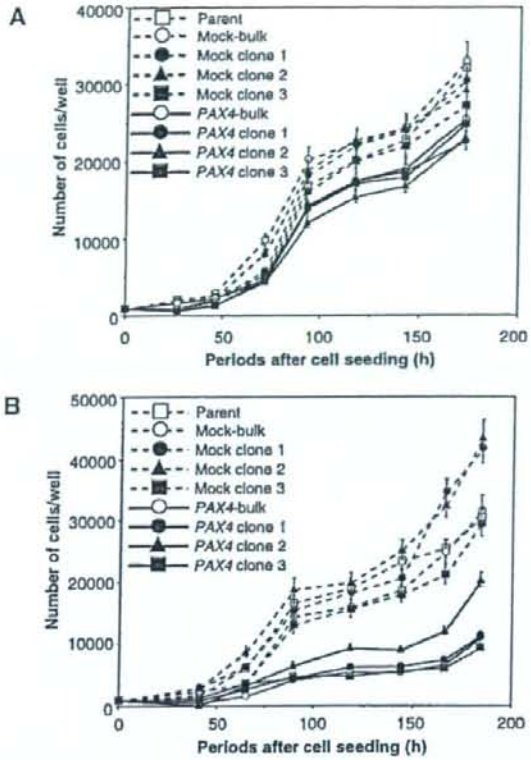

Figure 3. Cell growth of *PAX4*-overexpressing cell lines and the control cell lines. The cell number was converted from the data of the absorbance in colorimetric WST-8 assay. Data of the cell number are shown as mean ± standard deviation. The p-value was <0.01 in the comparison between any of *PAX4*-overexpressing cell lines and any of the control cell lines (parent and Mock) 93.5 h (C8161) (A) and 89 h (MeWo) (B) after the cell seeding (by one-way ANOVA followed by Scheffe's *F* analysis as a post-hoc test).

at 94˚C for 15 sec, an annealing step at 60˚C for 30 sec and an extention step at 72˚C for 1 min for 40 cycles. Primer concentrations of reactions of each *PAX* gene were 0.6 μM except 0.3 μM for *PAX7*. Data were analysed with Sequence Detector Systems version 2.0 software (Applied Biosystems). The copy number of PCR products (cDNA) was quantified by using the standard curve method. Standard curves were drawn in the same method described in our previous study (24). Expression levels of *PAX* genes were shown as the ratio of the target *PAX* gene to the internal reference gene (ß-actin) expression based on the initial copy number calibrated along the standard curve.

Cell growth assay. The number of viable cells was estimated by colorimetric WST-8 assay using the tetrazolium salt/formazan system (Dojindo, Kumamoto, Japan). Cell suspension (100 μl) (1x10⁴/ml, DME/F12-10% FBS) was placed in each well of a 96-well tissue culture plate. At intervals of 24 h after the cell seeding, 10 μl of WST-8 solution was added to the wells in a quadruplicate manner and incubated in a CO_2 incubator. After 1 h of incubation, absorbance of soluble formazan was measured at 450 nm wavelength (655 nm reference wave length) by using a Microplate reader (Bio-Rad Laboratory, Hercules, CA). The data are presented as the mean ± SD of quadruplicate wells.

Cell cycle analysis by flow cytometry. After cells were detached by the treatment with PBS (-) containing 0.2% trypsin and 2 mM EDTA, they were washed twice with PBS (-). Cells (1x10⁶) were fixed in 70% EtOH at room temperature for 1 h. After washing the cells with PBS, 100 μl of ribonuclease solution (100 μg/ml) was added to the cell pellet. After being kept at room temperature for 5 min, the cells were stained with 400 μl of propidium iodide (PI) solution (50 μg/ml) for evaluation of DNA content. Fluorescent intensity of PI was analysed by using FACS Calibur (Becton-Dickinson, San Jose, CA).

Assay for DNA synthesis. DNA synthesis was measured by means of 5-Bromo-2-deoxyuridine (BrdU) incorporation into cellular DNA with the use of colorimetric Cell Proliferation ELISA (BrdU) assay kit (Roche Diagnostics, Indianapolis, IN). Cells (1x10³/100 μl/well, DME/F12-10% FBS) seeded on 96-well tissue culture plate were incubated in CO_2 incubator for 24 h. The medium was replaced with DME/F12-10% FBS containing 10 μM BrdU. After BrdU-pulsing for 2 h, the cells were fixed and incubated with peroxidase-labelled anti-BrdU antibody. Then, tetramethyl-benzidine, a peroxidase substrate, was added to each well and the reaction was then stopped with 0.2 M H_2SO_4. Absorbance was measured at 450 nm wavelength (655 nm reference wave length) by using a Microplate reader. The data are presented as the mean ±SD of quadruplicate wells.